Auger intra-atomic transitions in grazing atom-surface collisions

M. Alducin
Departamento de Física de Materiales, Facultad de Química, UPV/EHU, Apartado 1072, 20080 San Sebastián, Spain

F. J. García de Abajo
Departamento Ciencias de la Computación e Inteligencia Artificial, Facultad de Informática, UPV/EHU, Apartado 649, 20080 San Sebastián, Spain

P. M. Echenique
Departamento de Física de Materiales, Facultad de Química, UPV/EHU, Apartado 1072, 20080 San Sebastián, Spain
(Received 1 November 1993)

The intra-atomic transitions involving bound states of an ion or an atom moving parallel to a solid surface are analyzed using linear-response theory. Different models have been employed to describe the response of the medium. The velocity dependence of excitation and deexcitation processes is studied. Numerical calculations are presented for transitions involving $1s$ and $2p$ hydrogenic states. The highest deexcitation rate is obtained when a $2p$ orbital is oriented in the direction normal to the surface. Numerical results are given for hydrogen atoms moving near aluminum. The decay of the deexcitation rate, which scales following a power law of the distance to the surface, proves to be almost independent of the velocity when $v<2$ a.u. The excitation probability is about two orders of magnitude below the deexcitation probability. Finally, the effect of the energy shift and splitting of the atomic states originating in the interaction with the valence-band electrons has been studied in detail.

I. INTRODUCTION

When an ion or an atom is moving parallel to a metal surface, the electrons of the probe can undergo transitions between bound states. The decay of an electron from an excited state is called Auger deexcitation (AD). Early attempts to analyze this process neglected many-body effects.[1-3] The role played by surface plasmons was investigated by Gersten and Tzoar.[4] More recently, Apell[5] showed that the mechanism of plasmon excitation is dominant in this case, that is, the excited projectile decays mainly by transferring its energy to the medium, giving rise to the creation of a plasmon. The effect has been studied for ion motion parallel with the surface using a local approximation to the response of the medium.[6,7] We extend these results in the present paper by using more reliable response functions with inclusion of dispersion. Moreover, we consider the Auger excitation (AE) and give a discussion of the effect that the splitting and mixing of the bound states, originating in the interaction with the surface, have on the transition rates.

The neutralization of an ion near a surface has contributions from different channels, including resonant[8,9] and Auger[10,11] processes. Oliphant and Moon, in their pioneering work,[12] pointed out that the capture to excited states and subsequent deexcitation could contribute significantly to charge exchange near a surface. In this way, Auger intra-atomic processes like those discussed in this work are relevant to the neutralization of ions near a surface.

The organization of this paper is as follows: in Sec. II we outline a theory of the problem; some numerical results are presented in Sec. III; Sec. IV is devoted to analysis of the influence of the screened potential on the states and levels of the probe. Atomic units (a.u.) will be used throughout this work.

II. THEORY

Let us consider an ion or an atom moving in vacuum parallel to a solid surface with velocity $\mathbf{v}$ at a distance z_0 from the jellium edge. The solid corresponds to the $z'<0$ region, where the z' direction is chosen perpendicular to the surface. The transition probability per unit time from the electron bound state $|\varphi_0\rangle$ to the state $|\varphi_1\rangle$ can be obtained by using first-order time-dependent perturbation theory. One finds

$$W_{10}=\frac{1}{\pi}\int_0^\infty d\omega\int_0^\infty \frac{d\mathbf{Q}}{Q}\delta(\omega-\mathbf{Q}\cdot\mathbf{v}+\Delta E)\,\mathrm{Im}\{g(Q,\omega)\}\times|\langle\varphi_1|e^{-i\mathbf{Q}\cdot\mathbf{R}}e^{-Q(z+z_0)}|\varphi_0\rangle|^2\,, \quad (1)$$

where ΔE is the energy difference between final and initial states, $\Delta E=E_1-E_0$, so that $\Delta E>0$ for AE and $\Delta E<0$ for AD. $g(Q,\omega)$ is the surface response function of the semi-infinite medium, which depends on the energy $\omega=\mathbf{Q}\cdot\mathbf{v}-\Delta E$ and the momentum Q transferred to the medium. This expression is similar to the one obtained when the ion moves fully inside the bulk material.[13] The origin of coordinates $(\mathbf{R},z)$ is chosen at the position of the ion. The conservation of energy is expressed through the δ function in Eq. (1), where $\mathbf{Q}\cdot\mathbf{v}$ represents the Doppler shift[6] due to the motion of the ion. It has been assumed in deriving Eq. (1) that the ion is located sufficiently far away from the surface so that the form factor, i.e., the term in angle brackets inside the squared

modulus in Eq. (1) involving the initial and final states, has negligible contributions from the region inside the solid (i.e., z_0 is much larger than the radii of the electron states).

The different form factors corresponding to each intra-atomic transition can be calculated analytically when the electron wave functions are of hydrogenic type, as explained in the Appendix. Notice that the expression e^{-Qz_0} included in the form factor of Eq. (1) acts like a cutoff for the momentum.

The well-known specular-reflection model (SRM), introduced in the study of the surface plasmon dispersion relation by Ritchie and Marusak[14] and independently discussed by Wagner,[15] will be used here to obtain the response of the surface. This model has been much used to calculate the induced surface potential.[16] In it, the surface response function reads

$$g(Q,\omega)=\frac{1-\varepsilon_s}{1+\varepsilon_s} , \tag{2a}$$

where

$$\varepsilon_s(Q,\omega)=\frac{Q}{\pi}\int \frac{dk_z}{k^2\varepsilon(k,\omega)} , \tag{2b}$$

and

$$k^2=Q^2+k_z^2$$

is the so-called surface dielectric function.[17] The calculation of ε_s involves the dielectric function of the bulk material, $\varepsilon(k,\omega)$. Two different approximations to the latter are used in the present work: (i) the plasmon-pole approximation (PPA)[18] and (ii) the random-phase approximation to the dielectric function[19] with the Mermin prescription,[20] which we shall refer to as the Mermin dielectric function (MDF). The latter incorporates a finite damping while keeping constant the number of electrons in the system. Apart from the SRM, two different approximations to the surface response function have been considered: (i) the classical frequency-dependent response function with damping,

$$g_0(\omega)=\frac{\varepsilon(\omega)-1}{\varepsilon(\omega)+1} , \tag{3}$$

where $\varepsilon(\omega)$ is the Drude dielectric function with finite damping

$$\varepsilon(\omega)=1-\frac{\omega_p^2}{\omega(\omega+i\gamma)} ; \tag{4}$$

and (ii) the Feibelman approximation,[21,22]

$$g_F(Q,\omega)=\frac{[\varepsilon(\omega)-1][1+Qd_p(\omega)]}{\varepsilon(\omega)+1-[\varepsilon(\omega)-1]Qd_p(\omega)} , \tag{5}$$

where $d_p(\omega)$ is the center of gravity of the screening charge induced by the external particle,[21-23] i.e.,

$$d_p(\omega)=\frac{\int dz\, z\rho^{\text{ind}}}{\int dz\, \rho^{\text{ind}}} . \tag{6}$$

The loss function $\text{Im}\{g(Q,\omega)\}$ presents a peak at the surface plasmon ($Q=0,\omega=\omega_s$).[24]

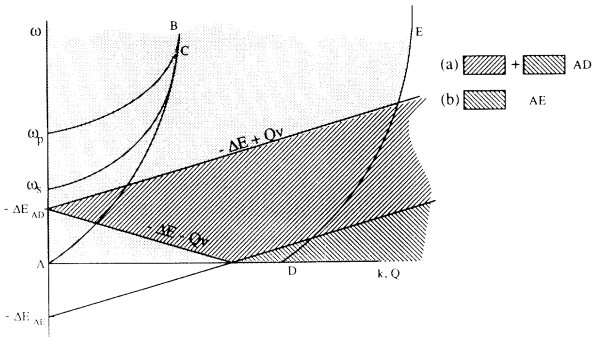

FIG. 1. Dashed zones representing the areas in the Q-ω plane in which the imaginary part of the surface response function $g(Q,\omega)$ is evaluated to compute Eq. (1), for Auger (a) deexcitation and (b) excitation. The curves ω_p and ω_s correspond to bulk and surface plasmon, respectively. The dotted area to the left of curve DE represents the surface spectrum of electron-hole pair excitations, whereas in the bulk this spectrum is limited by curves AB and DE. The surface and bulk plasmon lines intersect the Landau cutoff AB at the same point C.

Figure 1 represents the spectrum of excitations in both the bulk k-ω plane, and the surface Q-ω plane, when the MDF is used. In the absence of damping, collective excitation modes of the bulk lie along the plasmon line $\omega_p(k)$, and the electron-hole pair excitations correspond to the region between curves AB and DE.[25] On the other hand, the spectrum of excitations in the surface is given by the surface plasmon line $\omega_s(Q)$, and the single-particle region lies in the dotted area above curve ADE (remember that Q is the parallel momentum transfer). The δ function in Eq. (1) limits the region where the surface response is evaluated in the Q-ω plane according to

$$-\Delta E-Qv\le\omega\le-\Delta E+Qv .$$

This region is shown in Fig. 1 as a dashed area. The AE ($\Delta E>0$) and AD ($\Delta E<0$) are considered separately. In the $v\to 0$ limit the surface response is only evaluated at the points along the line $\omega=-\Delta E$. Therefore, AE is forbidden in that case, while AD can result in the creation of both electron-hole pairs and plasmons,[5] as long as the surface plasmon frequency is close to $-\Delta E$. Otherwise, the main contribution comes from electron-hole pairs.

III. RESULTS AND DISCUSSION

In this section, we focus on the Auger intra-atomic transition rates of hydrogen atoms moving close to an aluminum surface ($r_s=2.07$ a.u. and $\gamma=1.35$ eV). The static and velocity-dependent cases are considered separately for the deexcitation processes in Secs. III A and III B, respectively, and a brief comment is made on excitation in Sec. III C.

A. Static case

Figure 2 shows Auger deexcitation rates from the $2p_z$ to the ground state as a function of the distance to the

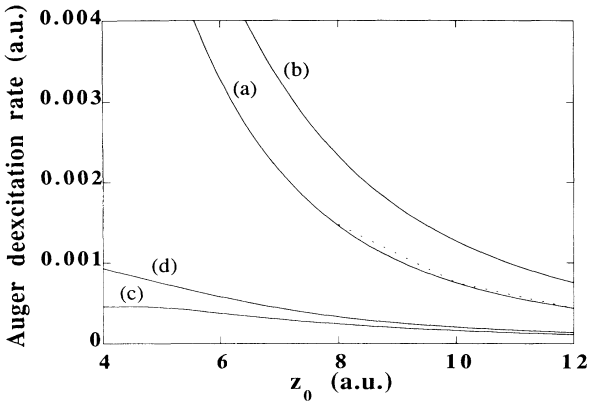

FIG. 2. Auger deexcitation rates in the static case ($v=0$) are represented versus atom-surface distance for $2p_z \rightarrow 1s$ transitions in H atoms using different surface response functions: (a) the classical response function with damping; (b) the Feibelman approximation; and the specular-reflection model together with (c) the plasmon-pole approximation, and (d) the Mermin dielectric function. A damping of $\gamma=1.35$ eV has been included in the dielectric functions. The surface under consideration is aluminum ($r_s=2.07$ a.u.). The dashed line corresponds to the asymptotic behavior given by Eq. (11).

surface. Different approximations to the surface response function have been considered: (a) the classical frequency-dependent response function with damping given by Eq. (3), (b) the Feibelman approximation,[21,22] and the SRM[14] together with (c) the PPA[18] and (d) the MDF[19,20] for the bulk response. Case (a) describes the response of the surface to an external perturbation through the surface plasmon line without dispersion. Case (b) is an approximation of the surface response function in the region of small momenta, which means for large atom-surface distances. Finally, cases (c) and (d) use the SRM according to which the surface susceptibility is expressed in terms of the bulk dielectric function while neglecting the interference effects between outgoing and reflected components of the electronic states of the electron gas.[26]

At small distances, the contribution to the Auger deexcitation rates mainly comes from the values that the surface response function takes at large Q, due to the exponential cutoff introduced by the form factor in Eq. (1). Consequently, the results obtained by using a surface response function will depend on whether dispersion is included or not. This explains the discrepancy of a factor of 5 between the probability obtained with the classical response function [curve (a)] and the one obtained by using the SRM with the MDF [curve (d)] at $z_0=6$ a.u. Nevertheless, one would expect that the probabilities should have a similar behavior at large distances, with a difference even smaller than the factor of 3 observed at $z_0=12$ a.u. between cases (a) and (d). The explanation for this difference can be found in the similar values of the energy transferred in the process under study, $\omega=-\Delta E=0.375$ a.u., and the surface plasmon frequency, $\omega_s=0.43$ a.u., so that the absence of dispersion in the classical response function, together with the broadening of the plasmon mode coming from the damping [case (a)], produces an overestimation of the effect of that collective excitation on the transition rate as compared to case (d). For this reason, the same calculation has been done for different surface parameters ($r_s=1.6$ a.u., that is, $\omega_s=0.60$ a.u.) but keeping $\gamma=1.35$ eV, so that the overlapping, due to the broadening introduced by the damping, between the surface plasmon line and the line along which the integral of Eq. (1) is performed is smaller than in the case of an aluminum surface. Figure 3 shows results for this case using the surface response functions (a) and (d) as in Fig. 2. (Notice that this conclusion has been extracted for a case in which $-\Delta E<\omega_s$. This is no longer true when $-\Delta E>\omega_s$, i.e., $r_s>2.2$ a.u. for H.) Now, the probability of Auger deexcitation has nearly the same behavior at large distances, independently of the model chosen to represent the response of the surface.

It is also noteworthy that the results show a strong dependence on the damping. The most extreme example is observed when the Drude response function is used: if a finite damping is considered, one obtains curves (a) in Figs. 2 and 3; however, if the damping is nearly zero, Eq. (1) reduces to

$$W_{10}=2\gamma\omega_s^2\int_0^\infty dQ\frac{-\Delta E}{(\omega_s^2-\Delta E^2)^2+(\gamma\Delta E)^2}\times|\langle\varphi_1|e^{-iQ\cdot R}e^{-Q(z+z_0)}|\varphi_0\rangle|^2 , \quad (7)$$

which vanishes in the $\gamma\rightarrow 0$ limit as long as the surface plasmon frequency is different from the transition energy.

A similar study has been carried out for the $2p_{x,y}\rightarrow 1s$ transitions. The results are qualitatively the same, although the probabilities are slightly smaller due to the fact that the electronic charge density of the $2p_z$ orbital is the closest to the surface and the form factor decays exponentially with z_0 for every Q.

For large values of $z_0(Q\ll 1)$, a good description of the form factors is provided by the dipolar approximation. In this case, the form factors are reduced to the following simple expressions in agreement with Ref. 6:

$$\langle 2p_x|e^{-iQ\cdot R}e^{-Q(z+z_0)}|1s\rangle\approx\frac{-iZ_1^4}{3\sqrt{2}}e^{-Qz_0}IQ_x , \quad (8)$$

$$\langle 2p_y|e^{-iQ\cdot R}e^{-Q(z+z_0)}|1s\rangle\approx\frac{-iZ_1^4}{3\sqrt{2}}e^{-Qz_0}IQ_y , \quad (9)$$

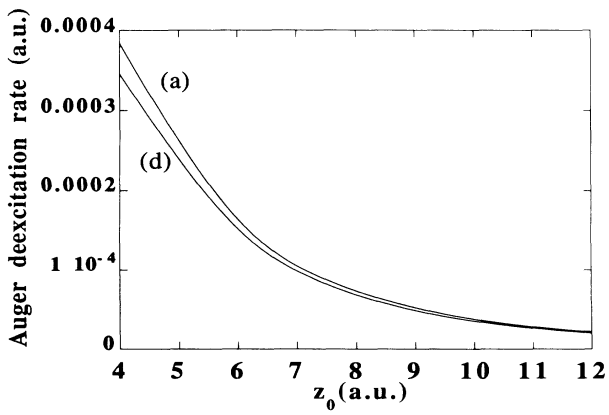

FIG. 3. As Fig. 2, but taking $r_s=1.6$ a.u. and $\gamma=1.35$ eV. All four response functions yield essentially the same result.

$$\langle 2p_z|e^{-i\mathbf{Q}\cdot\mathbf{R}}e^{-Q(z+z_0)}|1s\rangle \approx \frac{-Z_1^4}{3\sqrt{2}}e^{-Qz_0}IQ\ , \tag{10}$$

and

$$\langle 2s|e^{-i\mathbf{Q}\cdot\mathbf{R}}e^{-Q(z+z_0)}|1s\rangle \approx e^{-Qz_0}O(Q^2)\ , \tag{11}$$

where

$$I=\int_0^\infty r^4 e^{-(3/2)Z_1 r}dr=\frac{4!}{(1.5Z_1)^5}\ ,\quad Q=\sqrt{Q_x^2+Q_y^2}\ ,$$

and Z_1 is the atomic number.

In order to check the validity of the dipolar approximation in the calculation of the form factors, Auger deexcitation rates have been obtained by using Eqs. (8)–(10) instead of the exact expressions given in the Appendix. Comparison of these results with the ones obtained by using the analytical expressions for the form factor shows that the dipolar approximation is only good for $z_0 \geq 8$ a.u., so that we have preferred the use of the exact form factors in order to calculate the Auger transition rates shown throughout this work.

The expressions for the form factors obtained by using the dipolar approximation, together with the classical response function [Eq. (3)], allow us to derive the asymptotic behavior of the Auger deexcitation rates, in the limit of large distances, expressed in Eq. (1). One finds

$$\Gamma_{2p_{x,y}\to 1s}\approx\frac{Z_1^8 I^2}{18\pi}\,\mathrm{Im}\{g_0(-\Delta E)\}\int\frac{d\mathbf{Q}}{Q}e^{-2Qz_0}Q_{x,y}^2$$
$$=\frac{Z_1^8 I^2}{18}\,\frac{-\gamma\omega_s^2\Delta E}{(\omega_s^2-\Delta E^2)^2+\gamma^2\Delta E^2}\,\frac{1}{4z_0^3}\ , \tag{12}$$

and

$$\Gamma_{2p_z\to 1s}\approx\frac{Z_1^8 I^2}{18\pi}\,\mathrm{Im}\{g_0(-\Delta E)\}\int\frac{d\mathbf{Q}}{Q}e^{-2Qz_0}Q^2$$
$$=\frac{Z_1^8 I^2}{18}\,\frac{-\gamma\omega_s^2\Delta E}{(\omega_s^2-\Delta E^2)^2+\gamma^2\Delta E^2}\,\frac{1}{2z_0^3}\ . \tag{13}$$

This behavior is mainly determined by the square of the form factor, which behaves like $Q^2e^{-2Qz_0}$, so that the probabilities vary as $1/z_0^3$ for large z_0. In Fig. 2 the dashed line corresponds to the asymptotic behavior for the $2p_z\to 1s$ transitions given by Eq. (13). An excellent agreement is observed at large distances.

B. Velocity dependence

Figure 4 shows the results of calculations performed for $2p\to 1s$ transitions at three different atom-surface separations ($z_0=4$, 8, and 12 a.u.). The MDF has been used. Curves obtained at different distances have a similar shape in each transition. Thus, it is possible to approximate these results by a universal velocity-dependent curve multiplied by a factor which decays like a power of the distance to the surface. In all processes, the probability of Auger deexcitation has a maximum value at the velocity v_m for which the plasmon excitation begins to give a relevant contribution, that is, when the curve $\omega=Qv-\Delta E$ intersects the plasmon line. The expression for such a velocity is

$$v_m=\frac{\omega_c+\Delta E}{Q_c}\ , \tag{14}$$

and it is the resonance point (Q_c,ω_c) where the plasmon curves intersect the continuum of single-particle excitations in the Q-ω plane (see the point labeled C in Fig. 1). The value of v_m is 0.72 a.u. in the case under discussion. This result is in good agreement with the maxima observed in Fig. 4 for the $2p_x\to 1s$ and the $2p_z\to 1s$ transitions (dashed vertical line). The decay from the $2p_y$ state will be discussed below.

The three $2p\to 1s$ transition rates are compared in Fig. 5 when the atom is placed at a distance $z_0=8$ a.u. from the surface. The $2p_z\to 1s$ transitions are the most probable, because the $2p_z$ orbital is the closest to the surface and the form factor decays exponentially with z for every Q. Notice that at $v=0$ a.u. the probability for the $2p_z\to 1s$ transitions is twice the rate for the $2p_{x,y}\to 1s$ transitions, in good agreement with Eqs. (12) and (13). Comparing the results for $2p_x\to 1s$ and $2p_y\to 1s$ transitions, it is observed that the first is more probable for slow velocities ($v<1$ a.u.), while for faster velocities the second dominates. The explanation of this effect may be found in the different dependence on θ introduced by the

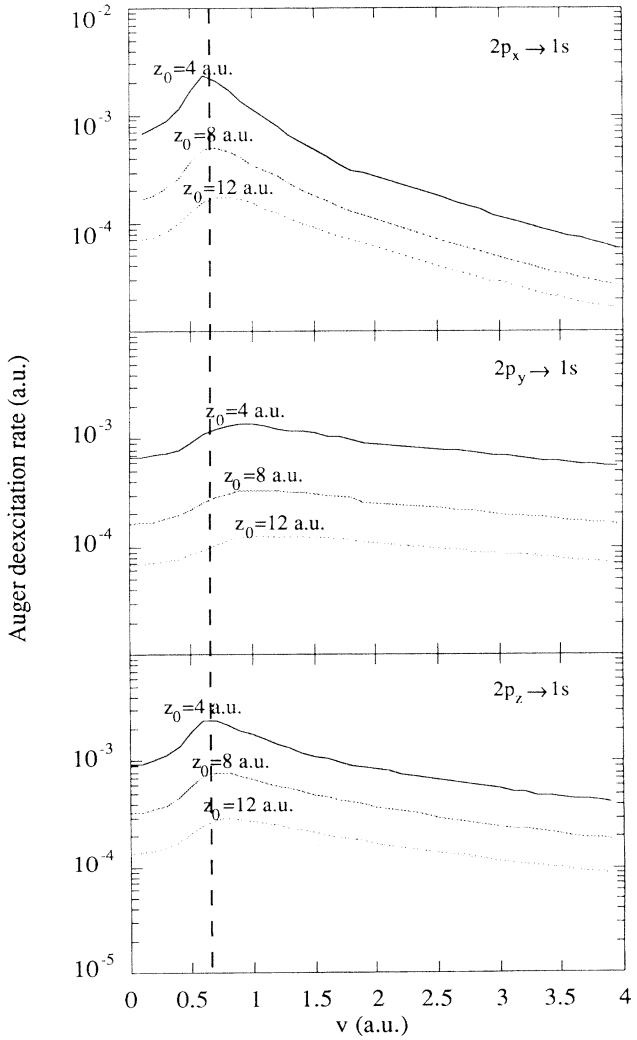

FIG. 4. Velocity dependence of the Auger deexcitation rate for $2p\to 1s$ transitions in H atoms moving parallel to an aluminum surface ($r_s=2.07$ a.u.). The probabilities have been calculated at three different distances to the surface: $z_0=4$, 8, and 12 a.u.

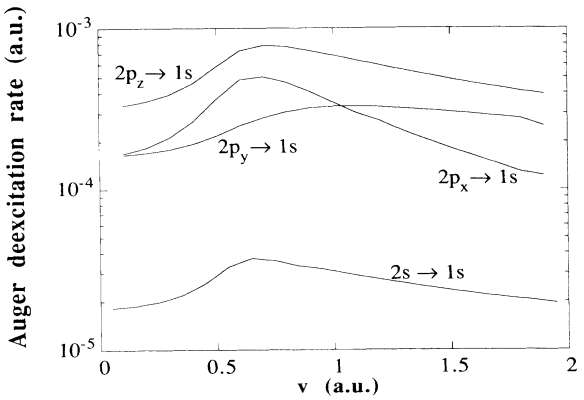

FIG. 5. Auger deexcitation rates versus atomic velocity for different transitions in H atoms moving parallel to an aluminum surface at a distance $z_0=8$ a.u. The Mermin dielectric function, together with the SRM, has been used.

form factor in Eq. (1), where θ is the angle formed by the parallel momentum $\mathbf{Q}$ and the atomic velocity $\mathbf{v}$ [see Eqs. (8) and (9)]. As was mentioned in Sec. II, the region where the surface response function is evaluated to calculate Eq. (1) corresponds to the points (Q,ω) that can satisfy the relation $\omega=Qv\cos\theta-\Delta E$ (the dashed area in Fig. 1). Thus, the $\cos^2\theta$ factor which appears in Eq. (1) for the $2p_x\rightarrow 1s$ transitions weights the surface response function in the sense that it enhances the contribution of the regions close to the straight lines $\omega=\pm Qv-\Delta E$, where θ is near the values 0, π, or 2π, instead of those in the neighborhood of $\omega=-\Delta E$, where θ goes to $\pm\pi/2$ (see Fig. 1). It is for low velocities that the surface plasmon line is located in the vicinity of $\omega=Qv-\Delta E$ (if $\omega_s>-\Delta E$ as it is the case in the problem under study), while for higher velocities it lies in the center of the hatched area. Consequently, the Auger $2p_x\rightarrow 1s$ deexcitation rates are enhanced by this geometrical consideration in the range of small velocities. However, in the $2p_y\rightarrow 1s$ transitions the $\sin^2\theta$ factor produces the opposite effect, so that the Auger rates in this case are larger for higher velocities, and the maxima are reached at slightly bigger velocities than the theoretical v_m (see Fig. 4). Calculations for $2s\rightarrow 1s$ transitions at $z_0=8$ a.u. show a probability in the range of 10^{-5}, for velocities below 2 a.u.

For large enough distances, the Auger deexcitation rates can be approximated by inserting the classical surface response function, Eq. (3), and the dipolar approximation to the form factors, Eqs. (8)–(10), into Eq. (1). In obtaining the asymptotic behavior of the Auger deexcitation rates for fast velocities, one finds a strong dependence on the damping as is the case for the self-energy.[27] Thus, when $\gamma\rightarrow 0$ one obtains the following expressions:[6]

$$\Gamma_{2p_x\rightarrow 1s}=\frac{Z_1^8 I^2}{18}\omega_s\frac{|\omega_s+\Delta E|^2}{v^3}K_0\left[\frac{2z_0|\omega_s+\Delta E|}{v}\right], \tag{15}$$

$$\Gamma_{2p_y\rightarrow 1s}=\frac{Z_1^8 I^2}{36}\omega_s\frac{|\omega_s+\Delta E|}{z_0 v^2}K_1\left[\frac{2z_0|\omega_s+\Delta E|}{v}\right], \tag{16}$$

and

$$\Gamma_{2p_z\rightarrow 1s}=\frac{Z_1^8 I^2}{18}\omega_s\frac{|\omega_s+\Delta E|^2}{v^3}\times\left[\frac{v}{2z_0|\omega_s+\Delta E|}K_1\left[\frac{2z_0|\omega_s+\Delta E|}{v}\right]+K_0\left[\frac{2z_0|\omega_s+\Delta E|}{v}\right]\right], \tag{17}$$

where K_0 and K_1 are the modified Bessel functions, which satisfy the asymptotic relation

$$K_n(x)\rightarrow\sqrt{\pi/2}\frac{e^{-x}}{x^{1/2}}\quad\text{for } x\gg 1\ . \tag{18}$$

Consequently, the asymptotic behavior of the Auger deexcitation rates, for distances such that $z_0\gg v/|\omega_s+\Delta E|$, is approximated by

$$\Gamma_{2p_x\rightarrow 1s}\approx\frac{Z_1^8\sqrt{\pi}I^2}{36}\frac{\omega_s|\omega_s+\Delta E|^{3/2}}{z_0^{1/2}}\frac{e^{-2z_0|\omega_s+\Delta E|/v}}{v^{5/2}}, \tag{19}$$

$$\Gamma_{2p_y\rightarrow 1s}\approx\frac{Z_1^8\sqrt{\pi}I^2}{72}\frac{\omega_s|\omega_s+\Delta E|^{1/2}}{z_0^{3/2}}\frac{e^{-2z_0|\omega_s+\Delta E|/v}}{v^{3/2}}, \tag{20}$$

and

$$\Gamma_{2p_z\rightarrow 1s}\approx\frac{Z_1^8\sqrt{\pi}I^2}{72}\omega_s\frac{|\omega_s+\Delta E|^{1/2}}{z_0^{3/2}v^{3/2}}\left[1+\frac{2z_0|\omega_s+\Delta E|}{v}\right]\times e^{-2z_0|\omega_s+\Delta E|/v}. \tag{21}$$

However, when γ is greater than zero, the asymptotic behavior is different:

$$\Gamma_{2p_x\rightarrow 1s}\approx\frac{Z_1^8 I^2}{18}\Delta\left[\frac{1}{8z_0^3}+\frac{3}{2}\left[\frac{\pi}{z_0}\right]^{1/2}\left[\frac{|\Delta E|}{v}\right]^{5/2}\times e^{-2z_0|\Delta E|/v}\right], \tag{22}$$

$$\Gamma_{2p_y\rightarrow 1s}\approx\frac{Z_1^8 I^2}{18}\Delta\left[\frac{1}{8z_0^3}-\frac{\sqrt{\pi}}{4}\left[\frac{|\Delta E|}{z_0 v}\right]^{3/2}\times e^{-2z_0|\Delta E|/v}\right], \tag{23}$$

and

$$\Gamma_{2p_z\rightarrow 1s}\approx\frac{Z_1^8 I^2}{18}\Delta\left[\frac{1}{4z_0^3}+\sqrt{\pi}\left[\frac{3}{2}\frac{Z_0|\Delta E|}{v}-\frac{1}{4}\right]\left[\frac{|\Delta E|}{z_0 v}\right]^{3/2}e^{-2z_0|\Delta E|/v}\right], \tag{24}$$

where

$$\Delta=\frac{-\gamma\omega_s^2\Delta E}{(\omega_s^2-\Delta E^2)^2+\gamma^2\Delta E^2}$$

and it has been assumed that $z_0 \gg v/|\Delta E|$. These last three equations are in good agreement with the dependence of the deexcitation rates shown in Fig. 5, which have been obtained by using a finite γ, on the velocity.

C. Auger excitation

A similar study has been performed for Auger excitation. We find that the excitation probabilities are about two orders of magnitude smaller than the deexcitation probabilities. Notice that the probability of excitation in the static case is zero,[5] because the energy transferred to the medium, ω, is negative [see Eq. (1)]. The dependence of the Auger excitation rate on the atomic velocity is shown in Fig. 6, at three different distances of the atom to the surface ($z_0=4$, 8, and 12 a.u.). The processes under consideration are: $1s \rightarrow 2p_x$, $1s \rightarrow 2p_y$, and $1s \rightarrow 2p_z$, corresponding to the upper, medium, and lower plots, respectively. Let us point out the existence of a threshold velocity

$$v_0=\frac{\Delta E}{2k_F}\ , \tag{25}$$

below which the transition probability must be zero in the absence of damping. This velocity is obtained when the line $\omega=-\Delta E+Qv$ cuts the curve DE in Fig. 1 which corresponds to the lowest edge of the region where single-particle excitations are possible. However, our results suggest a higher effective threshold velocity which depends on the distance to the surface. This effect is due to the peaked shape of $\mathrm{Img}(Q,\omega)$, whose highest values lie along and near the surface plasmon curve.[24] As the distance of the atom to the surface increases, the threshold velocity must be higher because $\mathrm{Img}(Q,\omega)$ has to be evaluated at $\omega \approx \omega_s$ in order to compensate the exponential cutoff e^{-2Qz_0} introduced by the square of the form factor in Eq. (1). [See the region (b) in Fig. 1 for Auger excitation.]

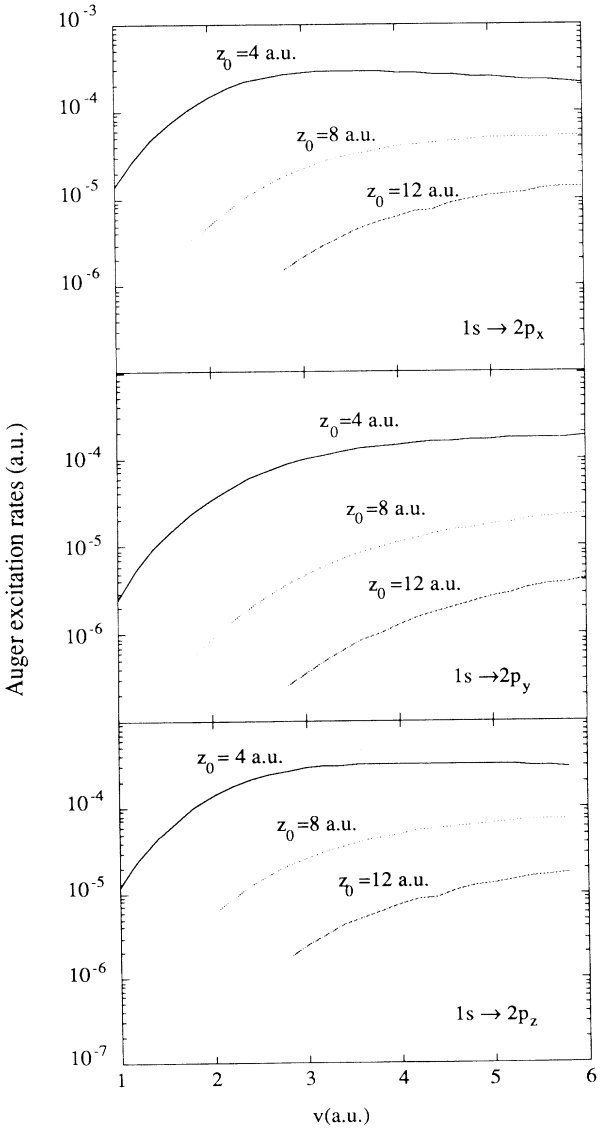

FIG. 6. As Fig. 4 for Auger excitation.

IV. EFFECT OF THE STARK SPLITTING ON THE TRANSITION RATES

The study of the Auger transition probabilities for an atom placed near a surface needs to take into account the perturbation introduced in the atomic levels and states by the surface-atom interaction through the induced potential. Some previous calculations go beyond linear response for the static case.[28,29] Since we are interested in the dynamic case as well, we will limit ourselves to the use of linear-response theory. This should be valid for obtaining a qualitative description of this effect, which will be referred to as the stark effect from now on. First-order perturbation theory has been applied to calculate the perturbed states of the atom. The total induced potential reads

$$V^{\mathrm{ind}}(\mathbf{R},z;\omega)=-\frac{Z_1}{2\pi}\int\frac{d\mathbf{Q}}{Q}e^{-Q(z+2z_0)}e^{-i\mathbf{Q}\cdot\mathbf{R}}g(Q,\omega)+\frac{1}{4\pi}\int\frac{d\mathbf{Q}}{Q}e^{-2Q(z+z_0)}g(Q,\omega)\ , \tag{26}$$

where the first term corresponds to the potential due to the image of the core in the solid and the second to the interaction of the bound electron with itself through the image potential. The electron coordinates $(\mathbf{R},z)$ are referred to the atomic nucleus.

The degeneracy of the $n=2$ level is totally removed in the dynamic case. The $2p_y$ level keeps roughly its unperturbed form. The rest of the states are hybrid and their expressions are

$$\begin{aligned}|\varphi_{s+p_z}\rangle&=a_1|2s\rangle+b_1|2p_z\rangle\pm c_1|2p_x\rangle\ ,\\ |\varphi_{s-p_z}\rangle&=a_2|2s\rangle-b_2|2p_z\rangle\pm c_2|2p_x\rangle\ ,\\ |\varphi_{p_x}\rangle&=a_3|2s\rangle+b_3|2p_z\rangle\pm c_3|2p_x\rangle\ ,\end{aligned} \tag{27}$$

where the coefficients depend on the velocity and the distance from the surface to the particle. The coefficients c_1, c_2, a_3, and b_3 increase with the velocity of the atom, and take values comparable to a_1, a_2, b_1, b_2, and c_3 for

$v \geq 1.5$ a.u.

In the static case, only two hybrid states are induced, i.e., $c_1 = c_2 = a_3 = b_3 = 0$, and the energetic degeneracy is only partially removed, because the shift in energy for states $2p_x$ and $2p_y$ is the same. We have used the SRM[14] together with the MDF[19,20] in order to evaluate the induced potential. This model allows us to calculate in a rather straightforward way the energy shifts and the perturbed states of hydrogen and alkali-metal atoms for intermediate and large distances. Besides, it allows us to study the Stark effect in the dynamic case.

In order to check the validity of our model, a comparison of our results for hydrogen in the static case with the ones obtained by a more sophisticated model[28] is illustrated in Fig. 7. In it, the variation of the energy for hydrogen levels $n=2$ and $n=1$ with the distance to an aluminum surface is represented. Solid lines correspond to the results obtained by the present model for levels (a) $1s$, (b) φ_{s-p_z}, (c) $2p_x$, and (d) φ_{s+p_z}. Similarly, dashed lines correspond to the results presented in Ref. 28 and (a') $1s$, (b') φ_{s-p_z}, (c') $2p_x$, and (d') φ_{s+p_z}. Both (a) and (a') are shifted 0.35 a.u. upward in the figure. For distances equal to or larger than 6 a.u., the energy shifts exhibit practically the same behavior in both models, except for the hybrid state φ_{s+p_z}. In this state, the electron density is shifted toward the surface, so that the state is more affected by the difference in the description of the potential in the points close to the surface. In any case, the Auger deexcitation rate depends on the difference of energy between the final and initial states, which is nearly the same in both models.

A. Static case

In the case of an atom at rest, the $2p_x$ and $2p_y$ levels suffer the same energy shift, since the system is invariant under rotation around the z axis. Figure 8 represents the

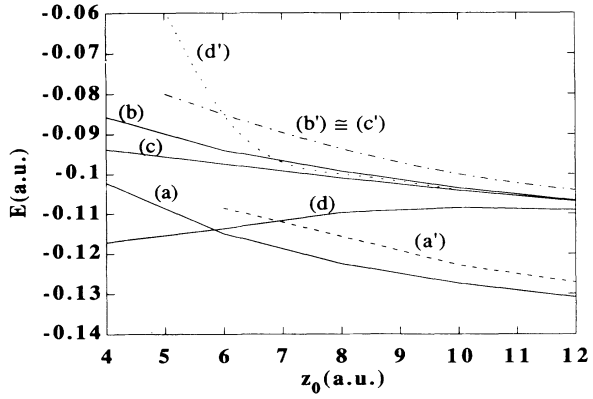

FIG. 7. Dependence of the energies of the hydrogenic levels $n=2$ and $n=1$ versus the atom-surface distance, when the H atom is at rest. Solid lines correspond to the energy obtained with the model described in the text for the levels (a) $1s$, (b) φ_{s-p_z}, (c) $2p_x$, and (d) φ_{s+p_z}. Dashed curves are taken from Norlander and Tully (Ref. 28) for levels (a') $1s$, (b') φ_{s-p_z} and $2p_x$, and (d') φ_{s+p_z}. Both (a) and (a') are shifted 0.35 a.u. upward in energy.

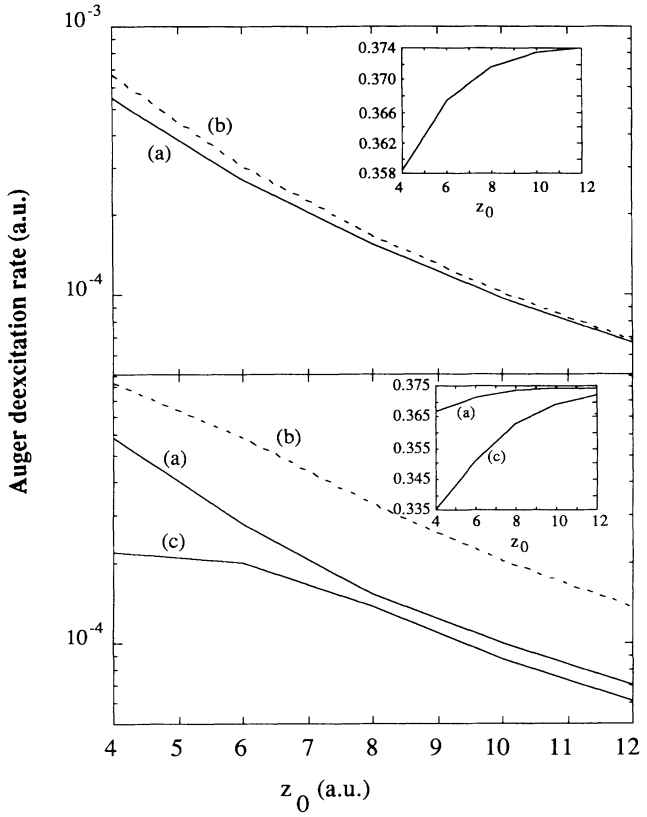

FIG. 8. Auger deexcitation rates in the static case as a function of the distance from the atom to the surface. The upper figure represents Auger probabilities for $2p_{x,y} \rightarrow 1s$ transitions, with (a) and without (b) inclusion of the Stark splitting. The lower figure shows the results obtained for transitions from hybrid states: (a) $s-p_z \rightarrow 1s$, (b) $2p_z \rightarrow 1s$ (unperturbed), and (c) $s+p_z \rightarrow 1s$. The inset in each figure represents the variation of the energy difference between initial and final states with the distance to the surface, i.e., $-\Delta E$ versus z_0.

Auger deexcitation rates for H in the vicinity of an aluminum surface as a function of the distance z_0. The upper figure corresponds to the $2p_{x,y} \rightarrow 1s$ deexcitations, either when the energy shift is introduced [curve (a)] or when no perturbation is considered [curve (b)]. By comparing these curves, one notices that the consequence of introducing the Stark effect is a decrease in the Auger deexcitation probabilities for small ion-surface distances ($z_0 < 8$ a.u.), whereas the correction introduced in the atomic levels hardly modifies the results for large distances. This is connected to the dependence of the transition energy, $\omega = -\Delta E$, on the distance (see the inset of Fig. 8). When the atom comes near the surface, both levels $n=2$ and $n=1$ are shifted upwards in such a way that the difference between the initial and final states, $-\Delta E(z)$, is smaller than if the Stark effect is not considered, $-\Delta E = 0.375$ a.u. Thus, the imaginary part of $g(Q,\omega)$ is evaluated at energies for which it takes smaller values as z_0 decreases. In the lower figure, curve (a) represents the $\varphi_{s-p_z} \rightarrow 1s$ transitions, curve (b) corresponds to the $2p_z \rightarrow 1s$ transitions, that is, if the Stark effect is not considered, and curve (c) stands for the

$\varphi_{s+p_z} \rightarrow 1s$ transitions. The introduction of the Stark effect again causes a decrease in the Auger deexcitation rate. Comparison between hybrid states makes it evident that the $\varphi_{x-p_z} \rightarrow 1s$ transitions are more probable than the $\varphi_{s+p_z} \rightarrow 1s$ transitions. The explanation could be found by comparing the energy transferred in the processes, $\omega = -\Delta E$, as has been done above for the $2p_{x,y} \rightarrow 1s$ transitions. However, their form factors have an important role also in the calculation of the Auger deexcitation rates. From the expressions obtained for the dipolar approximation in Eqs. (8)–(11), one has

$$|\langle 2s|e^{i\mathbf{Q}\cdot\mathbf{R}}e^{-Q|z+z_0|}|1s\rangle|^2 \ll |\langle 2p_z|e^{i\mathbf{Q}\cdot\mathbf{R}}e^{-Q|z+z_0|}|1s\rangle|^2 , \quad (28)$$

and therefore

$$|\langle 2p_z|e^{i\mathbf{Q}\cdot\mathbf{R}}e^{-Q|z+z_0|}|1s\rangle|^2 > |\langle \varphi_{s\pm p_z}|e^{i\mathbf{Q}\cdot\mathbf{R}}e^{-Q|z+z_0|}|1s\rangle|^2 . \quad (29)$$

Equation (29) could explain the difference observed between $\varphi_{s\pm p_z} \rightarrow 1s$ and $2p_z \rightarrow 1s$ deexcitations. Furthermore, comparing the overlapping of both φ_{s-p_z} and φ_{s+p_z} with the ground state, one concludes that the surface enhances transitions from the first state instead of the second one by means of the cutoff e^{-2Qz_0}.

B. Case $v \neq 0$

The influence of the velocity on the behavior of the Auger deexcitation rates has also been studied. In Fig. 9, the rate of Auger deexcitation from the level $n=2$ to the ground state is represented versus atomic velocity when the distance to the surface is 8 a.u. The dashed curves correspond to the Auger deexcitation rates obtained in Sec. III, when the Stark effect was not considered. In general, the probabilities of deexcitation are higher for the unperturbed states. The arguments that have been pointed out in the previous section can be applied here as well. The Auger deexcitation rates for the $\varphi_{p_x} \rightarrow 1s$ transitions are represented in the uppermost plot of Fig. 9, where curves (a) and (b) are obtained with and without inclusion of the Stark effect. The steep slope of curve (a) for high velocities is remarkable. This is due to the dependence of the energy difference between the initial and the final states $-\Delta E$ on the velocity. The probability of the $2p_y \rightarrow 1s$ transitions, represented in the middle plot, hardly suffers any variation by introducing the correction due to the Stark effect [curve (b)]. In the lowest plot, (c) corresponds to the $2p_z \rightarrow 1s$ transitions, obtained when the Stark effect is neglected, and (a) and (b) to the $\varphi_{s-p_z} \rightarrow 1s$ and the $\varphi_{s+p_z} \rightarrow 1s$ transitions, respectively. Similarly to the static case discussed above, the probability of Auger deexcitations is higher for the $\varphi_{s-p_z} \rightarrow 1s$ transitions than for the $\varphi_{s+p_z} \rightarrow 1s$ transitions. The reasons for this behavior are, as well, the dependence of $-\Delta E$ on the velocity, which is higher for the φ_{s-p_z} state,

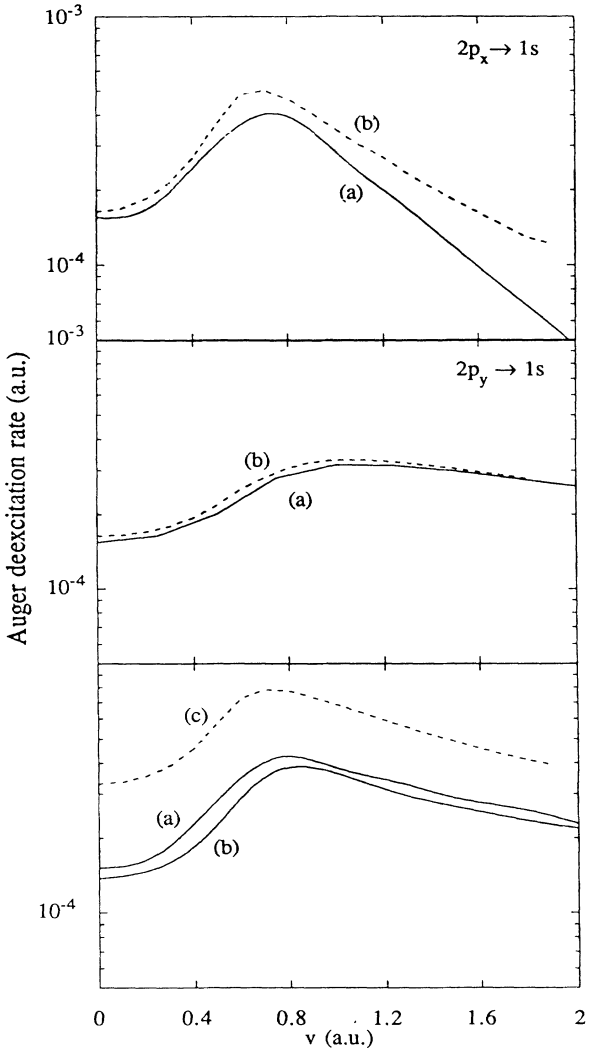

FIG. 9. Auger deexcitation rates as a function of the atom velocity when the particle is placed at 8 a.u. from the surface. Top: the $2p_x \rightarrow 1s$ transitions are plotted when the Stark effect is accounted for [curve (a)] and when it is not [curve (b)]. Middle: the same for $2p_y \rightarrow 1s$ transitions. Bottom: the same for hybrid states, (a) $s-p_z \rightarrow 1s$, (b) $s+p_z \rightarrow 1s$, and (c) $2p_z \rightarrow 1s$.

and the different overlapping with the ground state.

Finally, Fig. 10 compares all possible deexcitations between the levels $n=2$ and $n=1$ for H located at a distance of 6 a.u. from an aluminum surface. For small velocities, the deexcitations from the φ_{p_x} [curve (a)] and φ_{s-p_z} [curve (b)] states are the most probable, while in the regime of higher velocities, the $2p_y \rightarrow 1s$ deexcitation [curve (c)] is more probable than the others. The arguments expounded in Sec. III B to justify the influence of the velocity on the probabilities obtained for $2p_x \rightarrow 1s$ and $2p_y \rightarrow 1s$ deexcitations can be applied here as well when the initial states are the perturbed ones φ_{p_x} and $2p_y$. Curve (d) corresponds to deexcitation from the φ_{s+p_z} state.

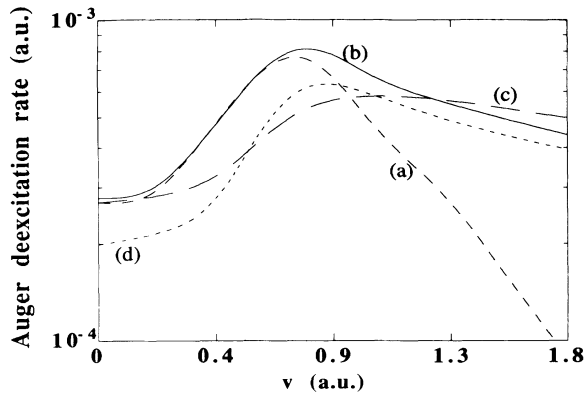

FIG. 10. Auger deexcitation rates have been represented for the four possible transitions between the levels $n=2$ and $n=1$. Curve (a) corresponds to $2p_x \rightarrow 1s$ transitions, curve (b) to $s-p_z \rightarrow 1s$, curve (c) to $2p_y \rightarrow 1s$, and curve (d) to $s+p_z \rightarrow 1s$. The distance from the atom to the surface is 6 a.u.

V. CONCLUSIONS

We have studied the Auger deexcitation processes between levels $n=2$ and $n=1$ induced in hydrogen atoms by the presence of an aluminum surface. In the static case, different approximations to the surface response function have been used. These results allow us to conclude that choosing a surface response function without dispersion results in overestimation of the contribution of the plasmon excitation in comparison with models where the dispersion is taken into account. At large distances, the Auger deexcitation rates are practically independent of the approximation used to calculate the surface response function. In all cases, their asymptotic behavior varies as $1/z_0^3$. Moreover, the value of the damping drastically affects the results.

Furthermore, we have extended the study of these processes to the case in which the H atom is moving with velocity parallel to the surface. The results show that the Auger deexcitation rates can be expressed for each $2p \rightarrow 1s$ transition as a universal velocity-dependent function multiplied by a factor which decays like a power of the distance to the surface. We have also found that the probability of Auger deexcitation has a maximum at the velocity for which the contribution of the plasmon excitations begins to be relevant, except in the case of $2p_y \rightarrow 1s$ transitions, where other geometrical considerations have to be taken into account, as was discussed in Sec. III B. Comparison of the different deexcitation processes between levels $n=2$ and $n=1$ shows that the most probable one corresponds to $2p_z \rightarrow 1s$ transitions.

A brief study has been performed for Auger excitation processes. The results indicate that the excitation probabilities are two orders of magnitude smaller than the deexcitation probabilities.

Finally, we have considered the perturbation induced in the atomic levels and states by the atom-surface interaction through the induced potential. Auger deexcitation rates to the ground states have again been calculated for this new situation. We find that the probabilities are smaller than those obtained previously, due to the energy shift and the new geometry of the eigenstates.

ACKNOWLEDGMENTS

The authors gratefully acknowledge partial financial support by the Spanish Government, Gipuzkoako Foru Aldundia, Eusko Jaurlaritza, and Iberdrola S. A. One of us (M.A.) also acknowledges a grant from the Basque government.

APPENDIX

The form factor in Eq. (1) can be analytically calculated when the electron wave functions which describe the initial and final states are hydrogenic wave functions. They can be expressed in terms of the derivatives of the function[30]

$$L(\alpha,q,\mathbf{G},z_0)=\int_0^\infty dz' \int d\mathbf{R}' e^{-qz'} e^{i\mathbf{G}\cdot\mathbf{R}'} e^{-\alpha|\mathbf{r}'-(0,0,z_0)|}$$

$$=2\pi\alpha\left\{\frac{4e^{-q|z_0|}\theta(z_0)}{(\Delta^2-q^2)^2}-\left[1+\Delta\left[\frac{1}{\delta}+|z_0|\right]\right]\frac{\mathrm{sgn}(z_0)e^{-\Delta|z_0|}}{\Delta^3\delta}\right\}, \tag{A1}$$

where $\Delta=\sqrt{\alpha^2+G^2}$ and $\delta=\Delta-q$. In the notation followed throughout this work, $\mathbf{r}'\equiv(\mathbf{R}',z')$ is referred to the jellium edge, while the origin of coordinates for $\mathbf{r}\equiv(\mathbf{R},z)$ is the ion core, so that $\mathbf{r}'=\mathbf{r}+(0,0,z_0)$. Notice that we have supposed the ion far away from the surface, so that the integral for $z'<0$ can be neglected. According to this, the form factor which describes the $2p_z \rightarrow 1s$ transition can be written

$$\langle 2p_z|e^{-i\mathbf{Q}\cdot\mathbf{R}}e^{-Q(z+z_0)}|1s\rangle$$

$$=\frac{Z_1^4}{4\pi\sqrt{2}}\int_0^\infty dz' \int d\mathbf{R}' e^{-(3/2)Z_1 r} e^{-i\mathbf{Q}\cdot\mathbf{R}} e^{-Q(z+z_0)} z$$

$$=\frac{Z_1^4}{4\pi\sqrt{2}} L_1(\tfrac{3}{2}Z_1,Q,-\mathbf{Q},z_0)\,, \tag{A2}$$

where

$$L_1(\alpha,q,\mathbf{G},z_0)=-\frac{\partial}{\partial\alpha}\left[\frac{1}{\alpha}\frac{\partial}{\partial z_0}L(\alpha,q,\mathbf{G},z_0)\right] . \quad \text{(A3)}$$

For the $2p_x \rightarrow 1s$ transition the form factor is

$$\langle 2p_x|e^{-i\mathbf{Q}\cdot\mathbf{R}}e^{-Q(z+z_0)}|1s\rangle = \frac{Z_1^4}{4\pi\sqrt{2}}\int_0^\infty dz'\int d\mathbf{R}' e^{-(3/2)Z_1 r}e^{-i\mathbf{Q}\cdot\mathbf{R}}e^{-Q(z+z_0)}x = \frac{Z_1^4}{4\pi\sqrt{2}}L_2(\tfrac{3}{2}Z_1,Q,-\mathbf{Q},z_0) , \quad \text{(A4)}$$

where

$$L_2(\alpha,q,\mathbf{G},z_0)=\frac{i}{G_x}\frac{\partial L(\alpha,q,\mathbf{G},z_0)}{\partial G_x} . \quad \text{(A5)}$$

Similarly, in the $2p_y \rightarrow 1s$ transition one obtains

$$\langle 2p_y|e^{-i\mathbf{Q}\cdot\mathbf{R}}e^{-Q(z+z_0)}|1s\rangle = \frac{Z_1^4}{4\pi\sqrt{2}}\int_0^\infty dz'\int d\mathbf{R}' e^{-(3/2)Z_1 r}e^{-i\mathbf{Q}\cdot\mathbf{R}}e^{-Q(z+z_0)}y = \frac{Z_1^4}{4\pi\sqrt{2}}L_3(\tfrac{3}{2}Z_1,Q,-\mathbf{Q},z_0) , \quad \text{(A6)}$$

where

$$L_3(\alpha,q,\mathbf{G},z_0)=\frac{i}{G_y}\frac{\partial L(\alpha,q,\mathbf{G},z_0)}{\partial G_y} . \quad \text{(A7)}$$

Finally, the form factor in the $2s \rightarrow 1s$ transition is given by

$$\langle 2s|e^{-i\mathbf{Q}\cdot\mathbf{R}}e^{-Q(z+z_0)}|1s\rangle = \frac{Z_1^3}{\pi\sqrt{8}}\int_0^\infty dz'\int d\mathbf{R}' e^{-(3/2)Z_1 r}e^{-i\mathbf{Q}\cdot\mathbf{R}}e^{-Q(z+z_0)}\left[1-\frac{Z_1}{2}r\right] = \frac{Z_1^3}{\pi\sqrt{8}}\left[L(\tfrac{3}{2}Z_1,Q,-\mathbf{Q},z_0)-\frac{Z_1}{2}L_4(\tfrac{3}{2}Z_1,Q,-\mathbf{Q},z_0)\right] , \quad \text{(A8)}$$

where

$$L_4(\alpha,q,\mathbf{G},z_0)=-\frac{1}{\alpha}\frac{\partial L(\alpha,q,\mathbf{G},z_0)}{\partial\alpha} . \quad \text{(A9)}$$

[1] H. S. W. Massey, Proc. Cambridge Philos. Soc. **26**, 386 (1930); **27**, 469 (1931); S. S. Shekter, Pis'ma Zh. Eksp. Teor. Fiz. **7**, 750 (1937); A. Cobas and W. E. Lamb, Jr., Phys. Rev. **65**, 327 (1944).

[2] H. D. Hagstrum, Phys. Rev. **96**, 336 (1954).

[3] C. W. White and N. H. Tolk, Phys. Rev. Lett. **26**, 486 (1971); W. R. van der Weg and D. J. Bierman, Physica (Utrecht) **44**, 206 (1969).

[4] J. I. Gersten and N. Tzoar, Phys. Rev. B **9**, 4038 (1974).

[5] P. Apell, J.Phys. B **21**, 2665 (1988).

[6] R. Zimny, Surf. Sci. **260**, 347 (1992).

[7] T. Iitaka and Y. H. Ohtsuki, Surf. Sci. **213**, 187 (1989).

[8] J. Los and J. J. Geerlings, Phys. Rep. **190**, 133 (1990).

[9] H. Winter, Comments At. Mol. Phys. **26**, 287 (1991).

[10] M. Alducin, A. Arnau, and P. M. Echenique, Nucl. Instrum. Methods Phys. Res. Sect. B **67**, 157 (1992); T. Fondén and A. Zwartkruis, Surf. Sci. **269/270**, 601 (1992); N. Lorente and R. Monreal, Nucl. Instrum. Methods Phys. Res. Sect. B **78**, 44 (1993).

[11] W. Sesselmann, B. Woratschek, J. Küppers, G. Ertl, and H. Haberland, Phys. Rev. B **35**, 1547 (1987); K. J. Snowdon, R. Hentschke, A. Närmann, and W. Heiland, Surf. Sci. **173**, 581 (1986).

[12] M. L. E. Oliphant, and P. B. Moon, Proc. R. Soc. London, Ser. A **127**, 338 (1930).

[13] P. M. Echenique, F. Flores, and R. H. Ritchie, in *Solid State Physics: Advances in Research and Applications,* edited by H. Ehrenreich and D. Turnbull (Academic, New York, 1990), Vol. 43, p. 229.

[14] R. H. Ritchie and A. L. Marusak, Surf. Sci. **4**, 234 (1966).

[15] D. Wagner, Z. Naturforsch. Teil A **21**, 634 (1966).

[16] R. Núñez, P. M. Echenique, and R. H. Ritchie, J. Phys. C **13**, 4229 (1980); P. M. Echenique, Philos. Mag. B **42**, L9 (1985); F. J. García de Abajo and P. M. Echenique, Phys. Rev. B **46**, 2663 (1992).

[17] D. M. Newns, Phys. Rev. B **1**, 3304 (1970).

[18] B. I. Lundqvist, Phys. Kondens. Mater. **6**, 206 (1967).

[19] J. Lindhard, K. Dan. Vidensk. Selsk. Mat. Fys. Medd **28**, (8) (1954).

[20] N. D. Mermin, Phys. Rev. B **1**, 2362 (1970).

[21] P. J. Feibelman, Prog. Surf. Sci. **27**, 438 (1982).

[22] P. Apell, Phys. Scr. **24**, 785 (1981).

[23] B. N. J. Persson and P. Apell, Phys. Rev. B **10**, 6058 (1983).

[24] See N. Zabala and P. M. Echenique, Ultramicroscopy **32**, 327 (1990), for a graphical description.

[25] D. Pines, *Elementary Excitations in Solids* (Benjamin, New York, 1963).

[26] F. García-Moliner and F. Flores, *Introduction to the Theory of Solid Surfaces* (Cambridge University Press, Cambridge, England, 1979).

[27] R. Nuñez, P. M. Echenique, and R. H. Ritchie, J. Phys. C **13**, 4229 (1980).

[28] P. Norlander and J. C. Tully, Phys. Rev. Lett. **61**, 990 (1988); Phys. Rev. B **42**, 5564 (1990).

[29] A. G. Borisov, D. Teillet-Billy, and J. P. Gauyacq, Nucl. Instrum. Meth. Phys. Res. Sect. B **78**, 49 (1993).

[30] J. W. Gadzuk, Surf. Sci. **6**, 133 (1967); A. Almulhem and M. D. Girardeau, *ibid.* **210**, 138 (1989).

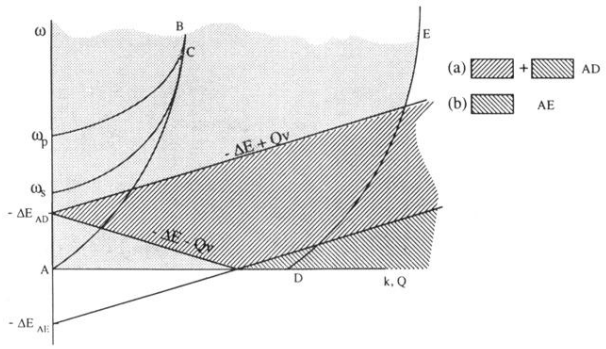

FIG. 1. Dashed zones representing the areas in the Q-ω plane in which the imaginary part of the surface response function $g(Q,\omega)$ is evaluated to compute Eq. (1), for Auger (a) deexcitation and (b) excitation. The curves ω_p and ω_s correspond to bulk and surface plasmon, respectively. The dotted area to the left of curve *DE* represents the surface spectrum of electron-hole pair excitations, whereas in the bulk this spectrum is limited by curves *AB* and *DE*. The surface and bulk plasmon lines intersect the Landau cutoff *AB* at the same point *C*.